

Beyond-mean-field fluctuations for the solution of constraint satisfaction problems

Niklas Foos,^{1,2,*} Bastian Epping,^{1,2,*} Jannik Grundler,^{1,2} Alexandru Ciobanu,^{1,2,3}
Ajainderpal Singh,⁴ Tim Bode,⁴ Moritz Helias,^{1,5} and David Dahmen^{1,†}

¹*Institute for Advanced Simulation (IAS6), Computational and Systems Neuroscience, Jülich Research Centre, Jülich, Germany*

²*RWTH Aachen University, Aachen, Germany*

³*Neuromorphic Compute Nodes (PGI-14), Peter Grünberg Institut (PGI), Jülich Research Centre, Jülich, Germany*

⁴*Institute for Quantum Computing Analytics (PGI-12), Jülich Research Centre, Jülich, Germany*

⁵*Department of Physics, RWTH Aachen University, Aachen, Germany*

Constraint Satisfaction Problems (CSPs) lie at the heart of complexity theory and find application in a plethora of prominent tasks ranging from cryptography to genetics. Classical approaches use Hopfield networks to find approximate solutions while recently, modern machine-learning techniques like graph neural networks have become popular for this task. In this study, we employ the known mapping of MAX-2-SAT, a class of CSPs, to a spin-glass system from statistical physics, and use Glauber dynamics to approximately find its ground state, which corresponds to the optimal solution of the underlying problem. We show that Glauber dynamics outperforms the traditional Hopfield-network approach and can compete with state-of-the-art solvers. A systematic theoretical analysis uncovers the role of stochastic fluctuations in finding CSP solutions: even in the absence of thermal fluctuations at $T = 0$ a significant portion of spins, which correspond to the CSP variables, attains an effective spin-dependent non-zero temperature. These spins form a subspace in which the stochastic Glauber dynamics continuously performs flips to eventually find better solutions. This is possible since the energy is degenerate, such that spin flips in this free-spin space do not require energy. Our theoretical analysis leads to new deterministic solvers that effectively account for such fluctuations, thereby reaching state-of-the-art performance.

I. INTRODUCTION

Constraint satisfaction problems (CSPs) play an important role in complexity theory and arise in various applications such as type inference in formal languages, coloring problems, scheduling, geometric modeling, cryptography, genetics, but also in logical puzzles, such as Sudoku [1–6]. Solving these problems requires finding variable assignments such that a minimal number of constraints are left unsatisfied. The MAX- K -SAT problem is one class of CSPs in which binary variables are combined in constraints of length $K \geq 2$, and the task is to find a variable assignment that satisfies a maximum amount of constraints.

The corresponding decision problem K -SAT is P (can be decided in polynomial time) for $K = 2$ and NP-complete for $K \geq 3$, a result that goes back to a classic paper by Karp [7]. Furthermore, 3-SAT can be reduced to MAX-2-SAT [8], proving that the latter is also NP-complete and thus cannot be solved in polynomial time unless it were shown that the NP class agrees to the class of problems solved in polynomial time [9, 10]. Many tools have been developed to solve these problems approximately.

For example, a classical line of works employs continuous Hopfield networks [11] and Boltzmann machines to find approximate solutions to CSPs such as the traveling salesman problem [12, 13]. To this effect, one maps the CSP to an Ising system, a model of interacting magnetic

spins pointing either up or down, and defines an energy function which is minimized by the configuration of spins that corresponds to the solution of the underlying CSP. Hopfield networks or Boltzmann machines are then used to find the (possibly degenerate) energy minimum (also called ground state) approximately. In Peterson and Anderson [14], the authors calculate the mean-field approximation of the Boltzmann machine, finding it both to be computationally cheaper and better performing, suggesting that a problem formulation in continuous variables simplifies the problem. In a similar manner, the same authors used the mean-field approximation of discrete Hopfield networks [15] to approximately solve the minimum cut bisection problem [16]. In Bilbro *et al.* [17], the mean-field approximation of the Ising formulation of a CSP was shown to be equivalent to the Hopfield network, and thus their performance is equivalent. Due to the good performance and its simple architecture, the continuous Hopfield network retains its relevance to this day [18–20].

In more recent studies, machine learning techniques such as graph neural networks have been used to develop better approximate CSP solvers (Selsam *et al.* [21], Toenschhoff *et al.* [22] and citations therein). While these models exist in many different versions, they operate on continuous spaces which are subsequently discretized to infer specific states of the given CSP. While these algorithms reach good approximate solutions, their progress and development is driven empirically and their architecture does not make use of the characteristics of the CSP's energy landscape.

While the aforementioned studies focus on developing efficient algorithms to find approximate CSP solutions, it

* Equal contribution

† Correspondence: d.dahmen@fz-juelich.de

is also worthwhile to investigate properties of the CSPs on their own. Insights into their structure may then be used to develop better solvers. In this vein, another line of works made use of methods from statistical physics developed for disordered systems, such as spin glasses, to investigate properties of the MAX- K -SAT problem as well as the decision problem, K -SAT [23–25]. This is done, as described for the above studies, by mapping the (MAX)- K -SAT problem to an Ising system, and identifying its energy function to represent the number of violated clauses for each variable/spin configuration. For (MAX)- K -SAT, this was first done in Monasson and Zecchina [26]. Studying MAX- K -SAT in the Ising setting using equilibrium statistical mechanics tools has proven fruitful, resulting in e.g. state-of-the-art approximate solvers [27–29] as well as estimates of the number of “good” solutions and quantifying the difficulty in finding them in dependence of the problem’s parameters [23, 26]. For random MAX- K -SAT problems, Monasson and Zecchina [26] investigated the phase transition when going from the underconstrained to the overconstrained regime of MAX- K -SAT, which occurs at a critical ratio between the number of constraints and the number of variables in the limit of infinitely large problems. A challenge shared among fixed-temperature solvers in the Ising formulation is choosing the temperature T to one that allows both to escape local minima and also to reach the ground state [25]. The probability of a state occurring is determined by the Boltzmann factor $e^{-\frac{E}{T}}$ where E is the energy of the state (setting the Boltzmann constant to one, $k_B = 1$). Thus, the system is expected to be in its ground state (or one of them, if the ground state is degenerate) if one were to set the temperature to zero. However, the approximations used to develop the solvers break at low temperatures, forbidding to go to the zero-temperature case.

In this work, we use Glauber dynamics [30] to simulate the Ising model. We find these discrete dynamics to outperform the traditional Hopfield-network approach on established benchmarks given by random MAX-2-SAT instances. Moreover, we find that the Glauber dynamics approach works best in the zero-temperature case, overcoming the limitation to finite temperatures of previous solvers. By employing a cumulant expansion of the Glauber dynamics [31] to investigate their properties, we find that Glauber dynamics in their mean-field approximation are equivalent to Hopfield networks. Including fluctuations in the form of the variances of individual spins allows us to identify free subspaces of spins in the phase space that are degenerate in energy; therefore no energy is needed to flip spins and explore these spaces. This happens even in the absence of thermal fluctuations due to the probabilistic nature of spin updates in the Glauber dynamics. From this variance approximation we obtain a new deterministic solver which reaches state-of-the-art performance on random MAX-2-SAT instances. In principle, our approach allows us to calculate the statistics of the Glauber dynamics to arbitrary order.

Here, we calculate the statistics up to the second cumulant and find a better match between simulated Glauber dynamics and its approximate version.

II. MAX-2-SAT AS A STATISTICAL PHYSICS PROBLEM

Formally, MAX-2-SAT problems consist of N binary variables $x_i \in \{0, 1\}$ where $i = 1, \dots, N$. Based on x_i we can define literals z_i which are either x_i or their negation $\bar{x}_i = 1 - x_i$. Clauses C_l with $l = 1, \dots, M$, also called constraints, are logical **OR**-connections of these literals, $C_l = \bigvee_{k=1}^K z_{i_{k,l}}$ where $z_{i_{k,l}}$ is the k -th literal in clause l with index $i_{k,l} \in \{1, \dots, N\}$. In this work we are concerned with MAX-2-SAT problems, meaning that in each clause there are at most two literals (we will exclusively use clauses of length two). As shown in Monasson and Zecchina [26] for the broader class of any (MAX-) K -SAT problem, this can be mapped to an Ising model by introducing spin variables $S_i = 2x_i - 1$, $i = 1, \dots, N$, corresponding to the Boolean variables x_i with value $S_i = 1$ in the case of $x_i = 1$ and $S_i = -1$ in the case of $x_i = 0$, respectively. The energy function of the resulting spin system can be written as

$$E(\mathbf{S}) = \frac{M}{4} - \sum_{i=1}^N H_i S_i - \frac{1}{2} \sum_{i,j=1}^N J_{ij} S_i S_j, \quad (1)$$

where the parameters H , J and M can be calculated from the clauses C_l in a straightforward manner [26] (see appendix A) by the condition that the energy $E(\mathbf{S})$ is the number of violated clauses in the MAX-2-SAT problem for the configuration that corresponds to the state \mathbf{S} . From here on, we will use the broader term CSPs to refer to MAX-2-SAT instances. Using the above mapping, solving a CSP is equivalent to finding the energy ground state in its corresponding spin system. This can be done approximately by using tools from statistical physics. In doing so one introduces an artificial temperature T and assigns probabilities $p(\mathbf{S}) \propto e^{-\frac{E(\mathbf{S})}{T}}$ to each state \mathbf{S} . We measure temperature in units of energy, such that the Boltzmann constant is $k_B = 1$. Then, one can approximate averages $\mathbf{m} = \langle \mathbf{S} \rangle$ (magnetizations) over this probability distribution. For solving CSPs, the most interesting temperatures are the ones close to zero, since in that case the system is most likely to be found in its ground state which in conclusion would dominate the average \mathbf{m} . In practice, however, approximate methods to find \mathbf{m} fail in the low temperature case due to the rough energy landscape with many local minima [32]. If one were to find the true magnetizations \mathbf{m} at zero temperature, these would give a state $\mathbf{S}^* = \mathbf{m}$ that would solve the CSP. Since it is NP-complete to solve the CSP, it thus is also NP-complete to find the magnetizations at zero temperature or to compute the partition function exactly

(since the magnetizations can easily be computed from the partition function).

A. Hopfield networks and Glauber dynamics

In this study, we focus on investigating and comparing mainly two different methods used to find the minimum energy state for the spin system written above. For one, we take the traditional Hopfield network approach [11]. This is a common approach for solving CSPs [20, 33–36]. In the original work [13], this has been used successfully for the traveling-salesman problem. For another, we will use Glauber dynamics [30] of the system (1) to sample states corresponding to minimal energy. Both methods are introduced in this section, starting with the Hopfield network.

In the continuous Hopfield model, variables model binary neurons ($S_i = +1$ and $S_i = -1$ for firing and non-firing neurons respectively) instead of spins. Then $m_i = \tanh(\beta\mu_i)$ takes the role of an average firing of neuron i which depends on its input voltage μ_i . We will find later that, when considering spin systems, $\mu_i(\mathbf{m})$ acts as an effective local field for spin i . The coupling matrix J_{ij} takes the role of synapses linking the neurons, feeding outputs S_i of neurons as inputs to other neurons while the variables H_i are to be interpreted as an external input to neuron i . The scaling factor β originates in biological details of the neurons and will later be identified with an inverse temperature. Using these naming conventions as well as neuron-independent time scales τ and \tanh as non-linearity, the Hopfield dynamics can be written as (see Appendix C for details)

$$\tau \frac{d\mu_i(t)}{dt} = -\mu_i(t) + \sum_{j=1}^N J_{ij} \tanh(\beta\mu_j(t)) + H_i. \quad (2)$$

These dynamics are monotonically decreasing the energy function (1) if one is to replace the spins $S_i \in \{-1, +1\}$ with the average firings $m_i \in [-1, +1]$ of the corresponding neurons. The solution strategy is thus to start from a random initialization of firings m_i and let the Hopfield network evolve until convergence, guaranteeing that one is in a local minimum of the energy function. However, one cannot determine from the time evolution whether this is the global minimum, or how close the energy one converged to is to the ground state energy. After convergence, the spin values are chosen as $S_i = \text{sign } m_i$. This is motivated by the fact that the energy of the CSP and the energy of the spin system (1) are the same for very high/low firing averages $m_i = \pm 1$.

The Glauber dynamics describe the physical evolution of the spin system introduced above [30]. They can be summarized as follows: In each time interval δt each spin S_i has the probability $\frac{1}{\tau}\delta t$ to be chosen for an update. Here τ denotes the time scale over which the system evolves. Throughout this manuscript all times are unitless i.e. considered relative to some unit time. If a spin i

is chosen for an update, we denote the probability of it being in the up state $S_i = 1$ or down state $S_i = -1$ after the update with $F^+(\mathbf{S}\setminus S_i)$ and $F^-(\mathbf{S}\setminus S_i) = 1 - F^+(\mathbf{S}\setminus S_i)$ respectively where $\mathbf{S}\setminus S_i$ denotes the set of all spins without the spin S_i . The expressions for $F^+(\mathbf{S}\setminus S_i)$ and $F^-(\mathbf{S}\setminus S_i)$ are given in Appendix D 1. As we are ultimately interested in the limit of infinitesimal small time intervals and the probability of two spins being updated in the same interval is $\propto \delta t^2$ only one spin at a time is updated at most. The net flux of probability in a state \mathbf{S} is given by the probability of another state changing into the state \mathbf{S} minus the probability of itself changing into another state. The flux can thus be decomposed into a sum of the probability fluxes of single spin flips

$$\tau \frac{d}{dt} p(\mathbf{S}, t) = \sum_{i=1}^N S_i \left(p(\mathbf{S}_{i-}) F_i^+(\mathbf{S}\setminus S_i) - p(\mathbf{S}_{i+}) F_i^-(\mathbf{S}\setminus S_i) \right). \quad (3)$$

Here, $p(\mathbf{S}, t)$ is the time-dependent probability distribution over the spins \mathbf{S} , and $\mathbf{S}_{i\pm}$ denotes the spin configuration \mathbf{S} with $S_i = \pm 1$. Since the Glauber dynamics describe a physical process, we can guarantee that this distribution is well behaved at all times t . While equation (3) captures the statistics of the Glauber dynamics, we can also simulate the dynamics as they are described above. To do this most efficiently, we make the following modification: We use the fact that at each time point only one spin will be updated. The time between two updates is, by definition of the Glauber dynamics above, an exponentially distributed random variable. During this time, spin configurations remain constant. Since we are only interested in finding the ground state spin configuration, we can speed up the simulation of the dynamics by imposing that in each time step exactly one randomly chosen spin is updated. This corresponds to the average behavior of the stochastic update described above for the choice $\tau = N\delta t$. To obtain a solution for a specific CSP we let the system equilibrate for a fixed time interval and subsequently measure the spins' magnetizations over another fixed time interval. The master equation (3) allows the theoretical investigation of these simulations which we will use to gain mechanistic insights on the role of fluctuations in section III.

In Figure 1 we show the result for both simulating the discrete Glauber dynamics and using the traditional approach of a continuous Hopfield network at low but non-zero temperature. Panel a) shows the spin evolution of the simulated Glauber dynamics. Starting from a random configuration, many spins flip their orientation shortly after the start of the simulation. At later times spins flip less frequently, but they do not fully freeze. The qualitatively same behavior can also be seen in panel b), showing the energy, or equivalently the number of violated clauses, as a function of time: For both the Glauber dynamics and the Hopfield network the energy drops rapidly after initialization and seems to converge for late times t where the energy of the simulation is eventually

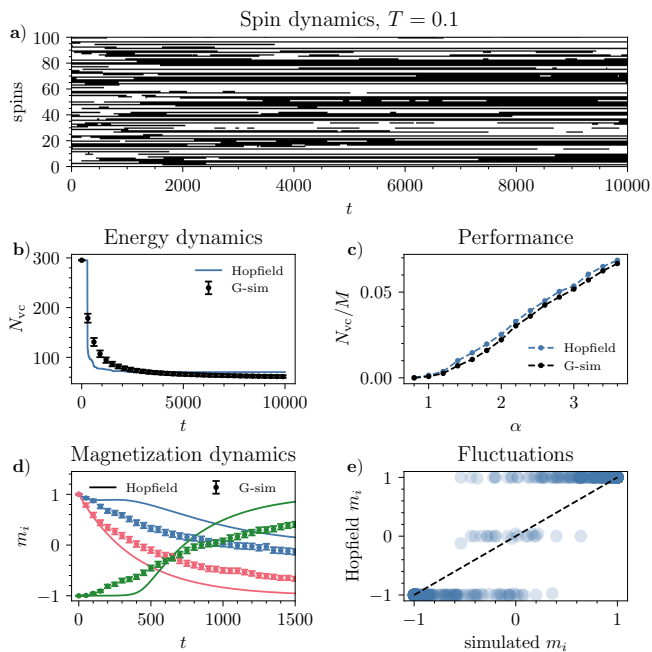


Figure 1. **Comparison of simulated Glauber dynamics and Hopfield networks.** a) Glauber spin dynamics in a random CSP with $\alpha = 3$ and $N = 400$. The evolution of a subset of $N = 100$ spins as a function of time starting from a random initialization. Black indicates a spin in the down state $S_i = -1$ while white indicates a spin in the up state $S_i = +1$. b) Energy as a function of time for one CSP instance and a single initial condition. c) Fraction of violated clauses dependent on clause density $\alpha = M/N$ averaged over 50 instances from a single random initial spin configuration. d) Magnetizations of three randomly chosen spins as a function of time t for Hopfield and Glauber dynamics (mean and standard deviation of the mean for 300 Glauber dynamics realizations) starting from the same initial condition. e) Magnetizations of spins in simulated Glauber dynamics and in the Hopfield network after convergence. All experiments in this figure are done with temperature $T = 0.1$. Details for CSP generation are provided in appendix B 1.

lower than that of the Hopfield network. The Glauber dynamics simulation thus found a better solution than the Hopfield dynamics in this specific CSP. To investigate the performance with better statistics, we show the performance of the two solvers for multiple instances with different clause densities in panel c). Interestingly the discrete Glauber dynamics outperform the continuous Hopfield network dynamics also here; they tend to find spin states violating less clauses than the Hopfield solution. The fraction of violated clauses for a wider range of α is shown in appendix F Figure A7. To gain first insights into how these solvers work, we show the magnetizations of three randomly chosen spins in both the Hopfield network and the Glauber dynamics in panel d). While the magnetizations are qualitatively similar, there are clear quantitative differences. In particular, the magnetizations in the Glauber dynamics are weaker,

implying that there the spins fluctuate more strongly. The magnetization in the Hopfield network on the other hand quickly freeze after some time in fully magnetized states. In panel e) we observe these spin magnetizations after convergence in both the Hopfield network and the Glauber dynamics. As in panel d) we observe similar magnetizations for most spins but also clear quantitative differences. Most prominently we notice that spins in the Hopfield network tend to be fully magnetized, while spins in the Glauber dynamics may obtain intermediate magnetization values.

The performance plot in panel b) finds the Glauber dynamics to be more performant, so seemingly the Glauber dynamics captures information of the underlying CSPs better. As we show in the next section, the performance difference can be explained by the stochastic spin fluctuations of the Glauber dynamics, leading to freely fluctuating spins with intermediate magnetizations which we already observed in panels d) and e). These fluctuations are absent in the Hopfield network which thus freezes the spins.

III. THEORETICAL ANALYSIS OF GLAUBER DYNAMICS

Next we analyze the Glauber dynamics to better understand how fluctuations shape the evolution of spin magnetizations and energies and how they may be beneficial for solving CSPs. Specifically, we perform a systematic cumulant expansion up to second order of the master equation (3). Taking into account all cumulants would result in the full Glauber dynamics including all random fluctuations, which guarantees the convergence of this expansion.

First, we apply a mean-field approximation in section III A, then move on to additionally include the variances of the spins while still discarding the cross-covariances in III B, and ultimately we perform the full expansion in the second cumulant in section III C.

A. Mean-field approximation

The simplest approximation of the Glauber dynamics is a mean-field approximation. In the mean-field approach one replaces the description of the probability distribution $p(\mathbf{S}, t)$ by a description of its mean values of the spins, $\mathbf{m}_i(t) = \langle \mathbf{S}(t) \rangle$, discarding all fluctuations. The mean-field approximation results in (for a derivation see appendix D 2)

$$\tau \frac{dm_i(t)}{dt} = -m_i(t) + \tanh(\beta \mu_i(t)), \quad (4a)$$

$$\mu_i(t) = H_i + \sum_j J_{ij} m_j(t). \quad (4b)$$

The dynamics of a mean value m_i are described by the right hand side of equation (4a) including a leak term

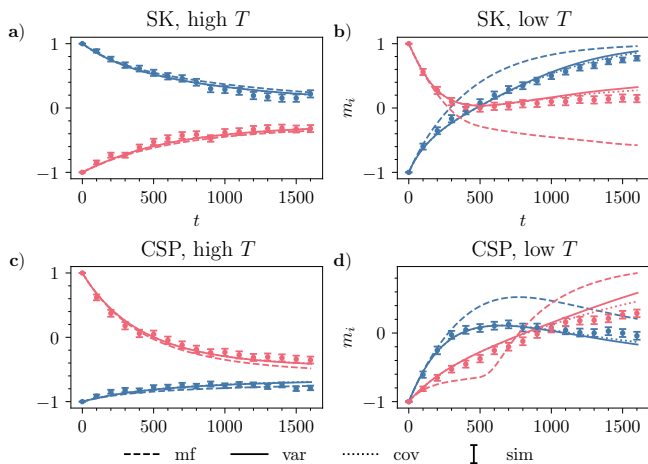


Figure 2. **Comparison of mean-field, variance and covariance approximations with simulated Glauber dynamics.** Magnetization of two spins as a function of time for simulated Glauber dynamics (mean and standard deviation of the mean over 300 trials) and solution for mean-field/variance/covariance equations. **a,b)** Sherrington-Kirkpatrick (SK) model instance at temperatures $T = 0.1$ and $T = 1$, respectively. **c,d)** CSP instance at temperatures $T = 0.1$ and $T = 1$, respectively. The first and second order statistics of the Gaussian couplings J_{ij} and fields H_i in the SK instance are matched to the corresponding statistics of the CSP instance. Parameters: $N = 400$, $\alpha = 3$.

and a local field (μ_i) term. In the absence of a local field, the leak term leads to exponentially vanishing magnetizations. The local field contains contributions from both the external field H_i of the spin S_i as well as an effective field generated by the other spins. These equations are equivalent to the continuous Hopfield dynamics, when written in the form of equation (2) (see appendix E).

This approximation has been very successful in the study of spin systems [32]. A prototypical example is the widely studied Sherrington-Kirkpatrick (SK) spin model [37], where spin couplings are independently and identically drawn from a Gaussian distribution $J_{ij} \stackrel{\text{i.i.d.}}{\sim} \mathcal{N}(J, J'/N)$. Here we additionally impose random external fields $H_i \sim \mathcal{N}(H, H')$ to mimic the structure of the CSP. The mean-field prediction shows good agreement with the Glauber dynamics in the SK system for high temperatures (Figure 2a). For low temperatures, however, theory and simulation deviate (Figure 2b). Indeed, the same behavior can be observed for CSPs with their sparse couplings: At high temperatures, the mean-field prediction and simulation agree (Figure 2c), but they disagree for small temperatures (Figure 2d). This mismatch between mean-field approximation and the full system for low temperatures, which we show quantitatively in appendix F Figure A8, is a common phenomenon. Disordered spin systems transition to a spin glass phase at low temperature with a complex energy landscape consisting of many local minima [38], in which particularly

the fluctuation-ignorant mean-field solver can get stuck. This explains the differences in performance between the deterministic Hopfield and stochastic Glauber dynamics in Figure 1, with the latter obtaining significantly better results at low temperatures.

Therefore we conclude that fluctuations described by higher-order statistics are important for solving CSPs at the required low temperatures. These fluctuations are not present in the Hopfield network, being equivalent to the mean-field approximation, thus explaining the worse performance. We include the higher-order fluctuations in the next sections.

B. Variance of spins: effective spin-dependent temperatures

The mean-field approximation only describes the first cumulant, the mean. Now we extend the mean-field description by the second cumulant. However, instead of taking the full second cumulant, the covariance, into account, we start by including only the variance of each spin, and include the full covariance in the next section. Given that the variance of binary variables is fully determined by their mean, this approximation still amounts to an equation for the means m_i only (see appendix D 3 for details)

$$\tau \frac{dm_i(t)}{dt} = -m_i(t) + \langle \tanh(\beta h_i) \rangle_{h_i \sim \mathcal{N}(\mu_i(t), \sigma_i^2(t))} \quad (5a)$$

$$\mu_i(t) = H_i + \sum_j J_{ij} m_j(t) \quad (5b)$$

$$\sigma_i^2(t) = \sum_j J_{ij}^2 (1 - m_j^2(t)). \quad (5c)$$

The average in equation (5a) is performed over a Gaussian random variable h_i (local field) with mean μ_i as in equation (4b) and with variance σ_i^2 . The fluctuations contained in this variance smear out the tanh non-linearity, while, in contrast, the mean-field approximation evaluates the non-linearity only at a single point. One obtains the mean-field approximation in the special case of vanishing variance $\sigma_i^2 = 0$.

Figure 2b and d show that the resulting prediction for spin magnetizations obtained by including the variance is accurate also at low temperatures. Moreover the temperature dependent performance of both the mean-field and the variance approximation together with the simulated Glauber dynamics in figure 3a shows two important aspects: 1) The best performance of both the simulation and the variance solver are found at vanishing temperature $T = 0$, while the mean-field solver is optimal at some intermediate temperature $T \approx 0.5$. This may seem counter intuitive since one may expect the solver to get stuck in local minima due to missing thermal fluctuations. We explain this phenomenon later in this section. 2) The best performance of the variance solver is significantly better than the one of the mean-field solver. In

fact, its performance is comparable to that of the simulation at all temperatures. Thus by including fluctuations one indeed obtains an accurate description of the simulated Glauber dynamics. This suggests that the qualitative difference between the Hopfield dynamics/mean-field approximation and the simulated Glauber dynamics are carried by the variance.

We explain these two findings in the following, starting with the temperature dependence. We observed that decreasing the temperature monotonically decreases the energy after convergence. Thus, we study the limit of zero temperature $T \rightarrow 0$ in the following. In this limit, the expectation value in (5a) reduces to an expectation value over the Heaviside step function which can be analytically calculated and results in

$$m_i = \operatorname{erf}\left(\frac{\mu_i}{\sqrt{2}\sigma_i}\right). \quad (6)$$

Interestingly, this result allows for weakly magnetized spins, i.e. spins with magnetization $m_i \neq \pm 1$, if the corresponding σ_i is non-zero. Fluctuations driving a non-zero σ_i appear in the Glauber dynamics simulation panel b) even for very large times and at $T = 0$ (Figure 3). Figure 3c shows the number of flips as a function of time. We find that shortly after initialization spins flip frequently. After some equilibration time the frequency of flips declines, but stays finite, such that continually spins are flipped. The dynamics of the spin flips after removing time steps in which no spin was flipped is shown in Figure 3d, while panel e) confirms that the variances of spins in the simulation are qualitatively correctly described by the variance solver for most neurons. Lastly panel f) shows the energy decay of the Glauber simulation and that in many cases spins are flipped although this does not result in an energy benefit. The explanation for this a priori puzzling finding can be found in the energy landscape of the underlying spin system: The energy function is degenerate, different spin configurations may have the same energy implying that the effective local field (4b) for these spins is vanishing. Thus, no energy (and therefore also no thermal drive) is needed to cause a spin to flip. In terms of the master equation (3) this implies that $F_i^+(\mathcal{S} \setminus S_i) = F_i^-(\mathcal{S} \setminus S_i)$ if for a flip of spin S_i the energy does not change (also see appendix D1 equation (D3)). If such a spin is chosen for an update, it flips with probability 1/2, being purely driven by the probabilistic nature of the Glauber dynamics.

These results suggest the following hypothesis: The continual flips allow the system to explore degenerate energy plateaus which helps finding better solutions with lower energy. While the flips themselves do not lower the energy, they freeze or unfreeze other spins, until eventually a spin is chosen that reduces the energy when flipped. The exploration of states of the same energy are observed as plateaus in Figure 3f. Since some spins are frozen at some times and unfrozen at other times they may have a magnetization which is both different from ± 1 and from

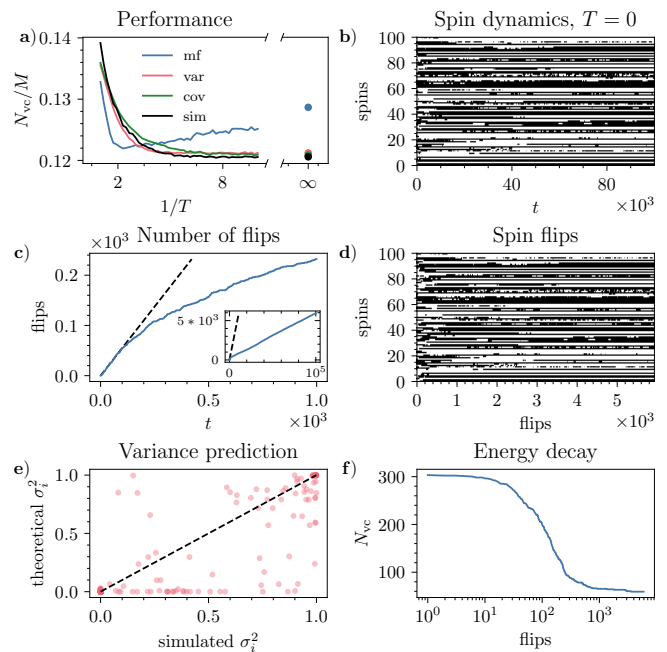


Figure 3. **Analysis of the variance solver.** **a)** Fraction of violated clauses as a function of inverse temperature $1/T$ for the mean-field, variance and covariance (see section III C) solver averaged over 50 CSP instances. **b)** Evolution of spin values over time (white: spin up, black: spin down) for simulated Glauber dynamics at $T = 0$ for one example CSP instance with $\alpha = 3$ and 100 randomly chosen spins. **c)** Number of spin flips as a function of time. The inset additionally shows later times and the black dashed line shows a linear fit for times shortly after initialization. **d)** Same as panel a) but dependent on spin flips instead of time. **e)** Simulated and theoretical prediction from the variance solver for variances σ_i^2 of spins. Variances of simulated dynamics are measured over $5 \cdot 10^4$ unit times after initialization at theoretical equilibrium state. **f)** Energy decay for simulated Glauber dynamics as a function of spin flips. Parameters: $N = 400$.

1/2. This effect and the resulting non-vanishing σ_i can be understood as an effective, spin dependent temperature. In the following, we will refer to spins which have such a non-zero temperature at a given time as free spins.

To test this hypothesis, we perform a perturbation experiment at temperature $T = 0$. Compared to the original system, the perturbed system has small additional random external magnetic fields $H_i \rightarrow \tilde{H}_i = H_i + \epsilon_i$ with $\epsilon_i \sim \mathcal{N}(0, 10^{-4})$. Due to this small perturbation, the energy degeneracy will be destroyed almost surely, and the effective local field (4b) will be non-zero. In the zero-temperature case, these small fields are sufficient to freeze the spins, prohibiting the aforementioned exploration of the energy landscape. Thus we expect the perturbed system to not exhibit any free spins, thus worsening the performance. The results of this experiment are shown in Figure 4. Panel a) confirms that at all times during the simulation there is a significant fraction of free spins. This fraction declines after initialization and converges to

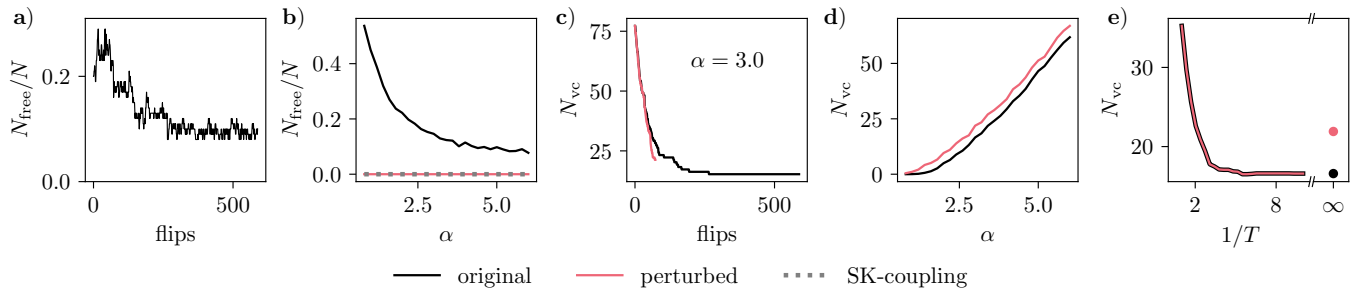


Figure 4. **Impact of a small perturbation on Glauber dynamics in a CSP instance.** **a)** Fraction of free spins in a CSP as a function of spin flips for zero temperature. **b)** Fraction of free spins as a function of clause density. Black line is for original CSP problems, red line for the corresponding perturbed CSPs with additional external field $\epsilon_i \sim \mathcal{N}(0, 10^{-4})$. The dotted gray line shows the fraction of free spins for an SK-coupling for the original case. The number of free spins was calculated after 10^4 time steps. **c)** Number of violated clauses as a function of spin flips for the simulated Glauber dynamics for both the original and the perturbed system of the same CSP as in a) at $T = 0$. **d)** Number of violated clauses as a function of the clause density both for the original and the perturbed CSP system at $T = 0$, calculated after 10^4 simulation steps. **e)** Number of violated clauses as a function of inverse temperature for the original and the perturbed system of the CSP from a). Parameters: $N = 400$, $\alpha = 3$.

a fixed value which depends on the clause density of the underlying CSP, as shown in panel b). Importantly there is a significant fraction of free spins at all clause densities if the system is unperturbed. A small perturbation, however, freezes all spins for arbitrary clause densities. Panel b) additionally shows the zero number of free spins for the dense, random SK coupling; free spins are thus resulting from the discrete and sparse nature of the CSP couplings, resulting in a relatively large probability that individual incoming inputs cancel each other and lead to a vanishing effective field.

Now we study the impact of this property on the solver’s performance by both observing the perturbed and unperturbed CSP system. Figure 4c shows the number of violated clauses (energy) as a function of spin flips. While the perturbed system lowers the energy with every spin flip and therefore its energy decays faster in the beginning in this display, all spins eventually become frozen and no more flips occur. It is thus impossible for the system to obtain a better solution, it is stuck in a local minimum. This is qualitatively different for the unperturbed system: At all times there is a fraction of free spins (see Figure 4a,b), allowing spin flips which do not change the energy. This leads to slower energy decay in the beginning when displayed as a function of spin flips, but allows exploration of the phase space at later flips, until eventually a better solution is found. The performance difference caused by this effect at $T = 0$ is shown in Figure 4d. Indeed, we observe significantly better performance for the unperturbed system for all clause densities. The temperature dependent performance for a fixed clause density is shown in Figure 4e: At finite temperature, the performance is comparable. In these cases, the non-zero thermal fluctuations are enough to overcome the small energy differences between states of the perturbed system; the perturbation thus does not qualitatively change the behavior. Only in the $T = 0$

case, the energy difference caused by the perturbation freezes the spins. At this point we thus observe a performance gap. We conclude that the energy degeneracy allows for spin flips even in the zero temperature case which help exploring the phase space and thus increase the performance of the Glauber dynamics solver.

We want to end this section with a short note on the computational complexity of the above discussed variance solver. In the $T = 0$ case we can use the analytic solution (6) for the expectation value in (5a) which leads to the same computational cost as the mean-field solver while obtaining a better performance. Moreover, we can use the insights from this section to speed up the Glauber dynamics simulation: Instead of choosing a spin at random for an update, we directly choose one of the free spins, since the frozen spins have probability zero to be flipped, even if they are chosen. Lastly we want to point out that these benefits only hold in the $T = 0$ case. At finite temperatures one would have to evaluate the integral in (5a) numerically.

C. Covariance of spins: expansion up to 2nd cumulant

Including the variance is only the first expansion term one can include on top of the mean-field approximation. In this section, we also include the next correction term, the covariance between spins. The time dynamics for this case are (derivation in appendix D 4)

$$\tau \frac{dm_i(t)}{dt} = -m_i(t) + \langle \tanh(\beta h_i) \rangle_{h_i \sim \mathcal{N}(\mu_i(t), \sigma_i^2(t))} \quad (7a)$$

$$\tau \frac{dc_{ij}(t)}{dt} = g(\mathbf{m}(t), \mathbf{c}(t)) \quad (7b)$$

$$\sigma_i^2(t) = f(\mathbf{m}(t), \mathbf{c}(t)) \quad (7c)$$

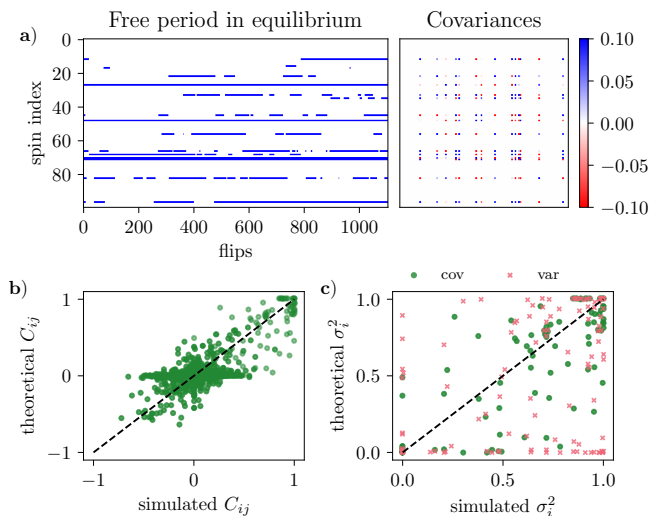


Figure 5. **(Co)variance comparison of theory and simulation.** **a)** Left: Frozen and free spins after equilibration as a function of flips at $T=0$. Free spins are marked in blue. Right: Empirical covariance matrix. Example of 100 spins. **b)** Scatter plot of theoretical and simulated covariance. **c)** Scatter plot of theoretical and simulated variance for both the variance solver (red) and covariance solver (green). Parameters: $N = 400$, $\alpha = 3$.

where the exact form of the functions f and g is stated in appendix D 4. Note that taking into account covariances amounts to an enlarged number of degrees of freedom due to the coupling between mean and covariances via (7c) and (7b).

We test the prediction of this expansion in Figure 5. In panel a) we show free periods of spins after equilibration in the Glauber dynamics simulation. These free periods amount to non-trivial coordinated fluctuations between spins as described by the covariance matrix of spins. These covariances are, to a good approximation, predicted by the covariance solver (Figure 5b). Moreover the prediction of variances is improved by including the covariances between spins (Figure 5c and Figure A9 in appendix F): While the variances are qualitatively correctly predicted by the variance solver we find quantitatively better agreement with the covariance solver. This makes sense, since including all orders would be a complete description of the simulated Glauber dynamics. In summary, the covariance solver describes the simulation quantitatively more accurately than the variance solver, but the variance solver is sufficient to describe the simulation qualitatively.

On the computational side, one may expect an increased performance from the covariance solver due to the additional degrees of freedom being the covariances between spins. Graph neural networks like RUN-CSP [22] profit from their high-dimensional phase space for solving CSPs. However, observing the performance of the covariance solver compared to the variance solver in Figure 3a we only find a minimal benefit for $T \rightarrow 0$, at

the expense of solving a set of $N + N(N - 1)/2$ equations instead of N equations for the variance solver.

IV. PERFORMANCE EVALUATION

Finally, we test the performance of the solvers investigated in this work, i.e. the Glauber-dynamics simulation (G-sim) as well as the solvers inspired by their approximation (G-mf, G-var and G-cov), and compare to other methods used in the literature, specifically a mean-field solver inspired by quantum mechanics, semi-definite programming, and a state-of-the-art graph neural network approach.

Quantum mean-field: The Mean-Field Approximate Optimization Algorithm (MF-AOA) was introduced in Misra-Spieldenner *et al.* [39] as a classical limit of the Quantum Approximate Optimization Algorithm (QAOA) [40]. In its continuous-time formulation [41], the MF-AOA leads to equations of motion very similar to (4a), the most notable difference being that the quantum mean-field lives on the Bloch sphere, i.e. instead of the classical $m_i(t)$ there are *three* degrees of freedom $\mathbf{n}_i(t) = (n_i^x(t), n_i^y(t), n_i^z(t))^T$ per spin. Note that it is natural to identify $m_i(t)$ with the z -component. The dynamics is given by precession in the effective magnetic fields $\mathbf{B}_i(t)$, described by the equations $\partial_t \mathbf{n}_i(t) = \mathbf{n}_i(t) \times \mathbf{B}_i(t)$, where $\mathbf{B}_i(t) = 2s_x(t)\hat{e}_x + 2s_z(t)\mu_i(t)\hat{e}_z$. The control fields $s_{x,z}(t)$ obey the boundary conditions $s_x(0) = s_z(t_f) = 1$ and $s_x(t_f) = s_z(0) = 0$. For the results shown in Figure 6, we set $t_f = 2^{10}$. The initial condition for the spins is $\mathbf{n}_i(t) = (1, 0, 0)^T$, from which the equations of motion are evolved up to time t_f . As above, the (approximate) solution to the optimization problem is finally obtained from the signs of the z -components.

Semidefinite programming: A classic result of computer science is the Goemans-Williamson (GW) algorithm [42] for the (weighted) MAX-CUT problem. By relaxing the Boolean variables x_i to the N -dimensional unit sphere, this problem is turned into a semidefinite program that can be solved by standard methods such as MOSEK interfaced in CVXPY [43]. Subsequently, the binary domain of the problem is recovered by a rounding mechanism, specifically by cutting the N -sphere with a random hyperplane. One advantage is that this algorithm comes with a performance guarantee of achieving ~ 0.878 of the optimal value, which also holds for MAX-2-SAT. In practice, when applied to any given problem instance, the algorithm often performs much better than this worst-case guarantee. For the special case of MAX-2-SAT, later results improve the GW value to ~ 0.935 by picking hyperplanes from a skewed distribution [44]. For the purpose of our work, we compare to this latter algorithm, which we denote by “SDP-skew” in Figure 6. Note that we show “single-shot” results, i.e. we pick a single hyperplane per random problem instance. This can be considered a fair comparison in the sense that we proceed similarly for the other algorithms. It does not take into

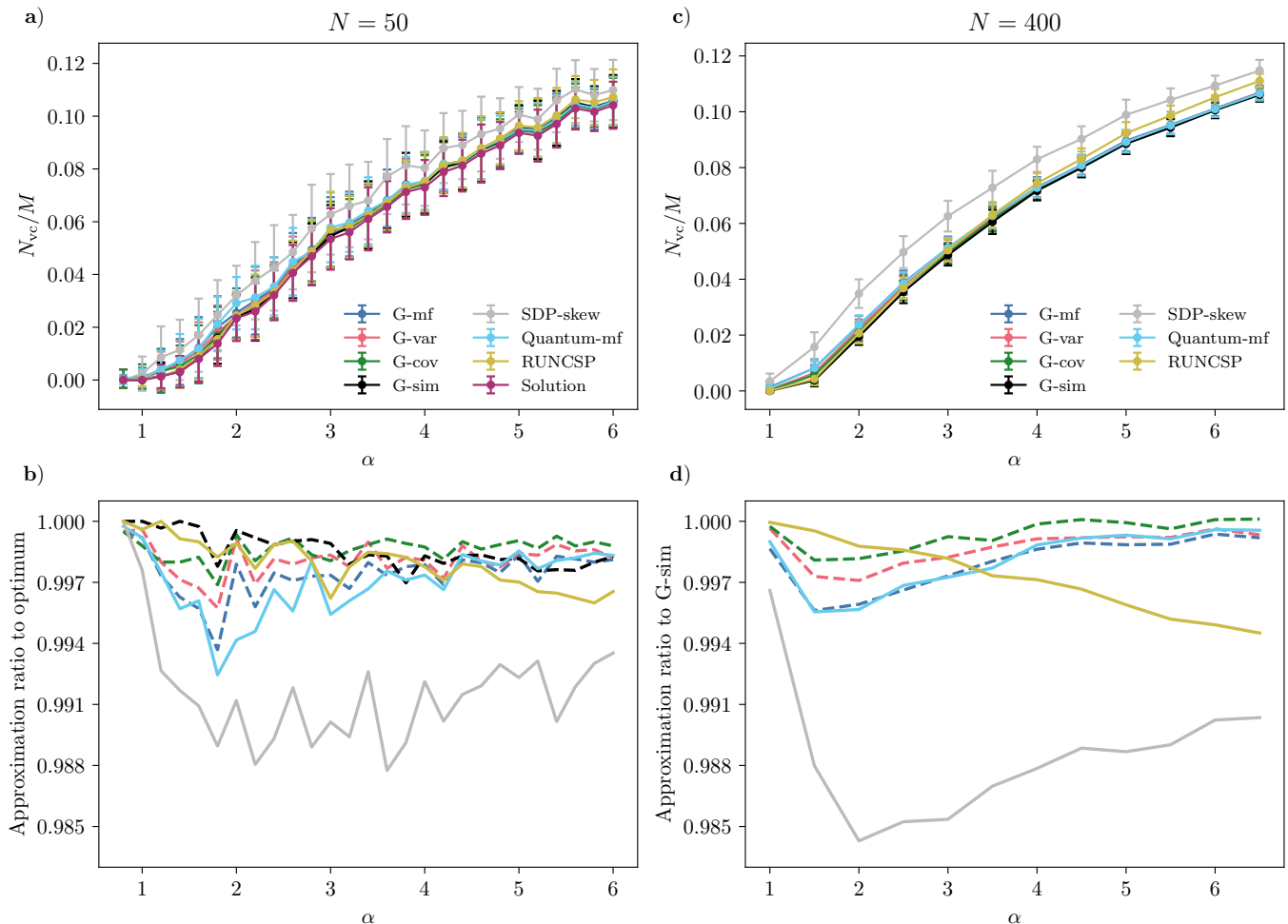


Figure 6. **Performance of all solvers.** For $N = 50$ (left column), the α values are chosen in the range 0.8 to 6.0 in steps of 0.2. For $N = 400$ (right column), the α values are in the range 1.0 to 6.0 in steps of 0.5. Markers show the mean and standard deviation across 50 instances per α and each solver has one random initial condition. The Glauber-based solvers are running at zero temperature except for the G-mf solver, which is running at its optimum $T = 0.5$ (cf. Figure 3a). **a)** Relative number of violated clauses as a function of clause density for $N = 50$. **b)** Mean number of violated clauses relative to the mean optimal number of violated clauses as a function of clause density. **c)** Relative number of violated clauses as a function of clause density for $N = 400$. **d)** Mean number of violated clauses relative to the mean violated clauses for the Glauber simulation as a function of clause density.

account runtime considerations, however.

Graph neural network (RUN-CSP): The graph neural network model RUN-CSP [22] functions by learning a message passing protocol in an unsupervised manner. Messages are passed only between literals/spins which participate in the same clause. The neural network architecture makes use of a high-dimensional state space (here $d = 128$) to store and process information of neighboring spins. A learnable projection determines the spin values of each spin from its high-dimensional representation.

Exact solution: Solving CSPs exactly takes exponential time and is thus only feasible for small instance sizes; this is the motivation to develop approximate solvers in the first place. However, it is valuable to compare the approximate solvers described above with the exact so-

lution on small instances, where the computing cost is manageable. To obtain the exact solution we use the RC2 MaxSAT solver from PySAT [45–47]. For larger system sizes where finding exact solutions becomes computationally infeasible we compare the approximate solvers among each other.

We show the result of the performance comparison in Figure 6 for small ($N = 50$) and large ($N = 400$) CSPs. Panel a) shows the fraction of violated clauses as a function of the clause density for small instances. The solution of all solvers, including the exact solutions, show the same qualitative trend: Below $\alpha = 1$, random MAX-2-SAT problems are almost always satisfiable [26], thus the number of violated clauses N_{vc} is zero. Increasing α , i.e., adding more and more constraints (while having the same number of spins) naturally increases N_{vc} , implying

that more and more clauses cannot be satisfied, even for the optimal solution. This trend is thus a property of the underlying CSPs and not a property of the solvers. The same trend can be observed for large instances (Figure 6b) where the exact solution is unfeasible to obtain due to the exponentially higher computational cost.

To better compare the solution of different solvers we also show the approximation ratio relative to the optimum for small instances (Figure 6c), and the approximation ratio relative to G-sim, as the best performing solver, for large instances (Figure 6d). For both small and large instances we find the Glauber-based solvers to match or slightly outperform the other state-of-the-art solvers. In most cases (except for the small instances and large clause densities) the simulation G-sim performs best, followed by G-cov, G-var and G-mf (being the Hopfield network). This is intuitive from the theoretical analysis above: Fluctuations are important to continue exploring the state space and finding better solutions. The more fluctuations we include into solvers, the better the obtained performance.

V. DISCUSSION

Solving CSPs is a fundamental problem in computer science and of practical importance in a wide range of applications. Due to their NP-completeness, often approximate solvers are used in practice for large instances. The research on approximate solvers is mainly driven by empirical work, resulting in strong solvers that are, however, often complex to interpret and analyze. Theoretical investigation of approximate solvers is of fundamental importance to find key similarities and to guide design choices.

In this study, we contributed to the understanding of approximate solvers by taking a statistical physics perspective on random MAX-2-SAT instances. Specifically, we investigated how Glauber dynamics, being a physical process of Ising-model dynamics [30], finds approximate solutions and compare this to the traditional Hopfield-network approach. We found the Glauber dynamics to outperform the Hopfield network, which corresponds to the mean-field approximation of the former, and identified statistical fluctuations as a key property for the high performance of solvers. Successively including fluctuations in a systematic manner results in more accurate descriptions of the Glauber dynamics and thus in stronger solvers.

Previous literature treating CSPs with statistical physics methodology concentrated on properties of the underlying problems, e.g. the transition from the solvable to non-solvable regime for random (MAX-)K-SAT problems Monasson and Zecchina [26] or describing how and why problems near this and other transitions are hard to solve, even approximately [48]. In our work, we use the Ising description of a CSP to design explicit solvers that find approximate solutions. Specifically, our solvers

are able to make use of the degenerate energy landscape that is typical for disordered systems such as MAX-2-SAT problems to explore different states and find better solutions. The main findings of our work are twofold: First, we obtain a series of systematic approximations of the Glauber dynamics, each of which mapping to a set of ordinary deterministic differential equations. These effective equations can hence be implemented with the same hardware [49–51] as traditional Hopfield networks, while reaching considerably higher performance. Second, we identify the physical mechanism that underlies this increased performance which is reached in the $T \searrow 0$ limit: The appearance of “free spins”, which are spin variables that feel a vanishing mean-field from their peers. Switching such variables does not change energy so they encode the macroscopically degenerate states in the energy landscape. By including their statistical fluctuations our algorithms efficiently explore this landscape, and thus ultimately find a better solution.

The strongest limitation of our work in its current form is that we only consider MAX-2-SAT instances, a specific class where the decision variant of the problem is solvable in polynomial time. An extension to other CSPs, such as $K > 2$ -SAT is an exciting and promising direction of future research: The key property of the MAX-2-SAT instances used in this work was the degeneracy of the energy landscape, which results from the discrete-valued couplings and magnetic fields in the Ising system. Since CSPs are discrete in nature, we hypothesize that the degenerate energy landscape is a property shared by many classes of CSPs, enabling a similar analysis as done here. Likewise, the employed method to derive effective deterministic equations of motion from a cumulant hierarchy is completely general and carries through to $K > 2$ -SAT problems with minor adaptations.

Another direction of future research is to use the covariance of spins in the solver more directly. Instead of picking each spin for update with the same probability, as in the classical Glauber dynamics, one could focus on those spins j that are correlated to spin i after a flip of spin i . The correlation makes it more likely for spin j to decrease the energy with another flip. Our method obtains approximations of this covariance, thus opening the door for such correlation-informed cluster update schemes.

In summary, our analysis provides a systematic formalism for the theoretical analysis of energy minimization and CSP optimization, and paves the way to systematically construct physics-based solvers that combine performance with interpretability.

Acknowledgments

This work was partially supported by the German Federal Ministry for Education and Research through BMBF Grant 01IS19077A to Jülich and via the funding program quantum technologies – from basic research

to the market – under contract number 13N15680 “GeQ-CoS”. Open access publication funded by the Deutsche

Forschungsgemeinschaft (DFG, German Research Foundation) – 491111487.

-
- [1] B. C. Pierce and D. N. Turner, Local type inference, *Acm transactions on programming languages and systems (toplas)* **22**, 1 (2000).
- [2] J.-X. Ge, S.-C. Chou, and X.-S. Gao, Geometric constraint satisfaction using optimization methods, *Computer-Aided Design* **31**, 867 (1999).
- [3] P. Hell and J. Nešetřil, Colouring, constraint satisfaction, and complexity, *Computer Science Review* **2**, 143 (2008).
- [4] L. Aceto, J. A. Hansen, A. Ingólfssdóttir, J. Johnsen, and J. Knudsen, The complexity of checking consistency of pedigree information and related problems, *Journal of Computer Science and Technology* **19**, 42 (2004).
- [5] A. Ramamoorthy and P. Jayagowri, The state-of-the-art boolean satisfiability based cryptanalysis, *Materials Today: Proceedings* **80**, 2539 (2023), sI:5 NANO 2021.
- [6] S. C. Brailsford, C. N. Potts, and B. M. Smith, Constraint satisfaction problems: Algorithms and applications, *European journal of operational research* **119**, 557 (1999).
- [7] R. M. Karp, Reducibility among combinatorial problems, in *Complexity of Computer Computations: Proceedings of a symposium on the Complexity of Computer Computations, held March 20–22, 1972, at the IBM Thomas J. Watson Research Center, Yorktown Heights, New York, and sponsored by the Office of Naval Research, Mathematics Program, IBM World Trade Corporation, and the IBM Research Mathematical Sciences Department*, edited by R. E. Miller, J. W. Thatcher, and J. D. Bohlinger (Springer US, Boston, MA, 1972) pp. 85–103.
- [8] M. R. Garey, D. S. Johnson, and L. Stockmeyer, Some simplified np-complete problems, in *Proceedings of the sixth annual ACM symposium on Theory of computing* (1974) pp. 47–63.
- [9] O. Goldreich, *P, NP, and NP-Completeness: The basics of computational complexity* (Cambridge University Press, 2010).
- [10] R. Garey Michael and S. Johnson David, *Computers and intractability: A guide to the theory of np-completeness* (1979).
- [11] J. J. Hopfield, Neurons with graded response have collective computational properties like those of two-state neurons, *Proc. Natl. Acad. Sci. USA* **81**, 3088 (1984).
- [12] C.-K. Looi, Neural network methods in combinatorial optimization, *Computers & Operations Research* **19**, 191 (1992).
- [13] J. J. Hopfield and D. W. Tank, Neural computation of decisions in optimization problems, *Biological Cybernetics* **52**, 141 (1985).
- [14] C. Peterson and J. R. Anderson, A mean field theory learning algorithm for neural networks, *Complex Syst.* , 995 (1987).
- [15] J. J. Hopfield, Neural networks and physical systems with emergent collective computational abilities, *Proc. Natl. Acad. Sci. USA* **79**, 2554 (1982).
- [16] C. Peterson and J. R. Anderson, Neural Networks and NP-complete Optimization Problems; A Performance Study on the Graph Bisection Problem, *Complex Systems* (1988).
- [17] G. Bilbro, R. Mann, T. Miller, W. Snyder, D. van den Bout, and M. White, Optimization by Mean Field Annealing, in *Advances in Neural Information Processing Systems*, Vol. 1 (Morgan-Kaufmann, 1988).
- [18] U.-P. Wen, K.-M. Lan, and H.-S. Shih, A review of hopfield neural networks for solving mathematical programming problems, *European Journal of Operational Research* **198**, 675 (2009).
- [19] S. Sathasivam, M. A. Mansor, M. S. M. Kasihmuddin, and H. Abubakar, Election algorithm for random k satisfiability in the hopfield neural network, *Processes* **8**, 568 (2020).
- [20] M. S. M. Kasihmuddin, S. Sathasivam, and M. A. Mansor, Hybrid genetic algorithm in the hopfield network for maximum 2-satisfiability problem, *AIP Conference Proceedings* **1870**, 050001 (2017).
- [21] D. Selsam, M. Lamm, B. Bünz, P. Liang, L. de Moura, and D. L. Dill, Learning a SAT solver from single-bit supervision, in *International Conference on Learning Representations* (2019).
- [22] J. Toenshoff, M. Ritzert, H. Wolf, and M. Grohe, Graph neural networks for maximum constraint satisfaction, *Frontiers in artificial intelligence* **3**, 580607 (2021).
- [23] M. Mézard, G. Parisi, and R. Zecchina, Analytic and algorithmic solution of random satisfiability problems, *Science* **297**, 812 (2002), <https://www.science.org/doi/pdf/10.1126/science.1073287>.
- [24] R. Monasson and R. Zecchina, Entropy of the k-satisfiability problem, *Physical review letters* **76**, 3881 (1996).
- [25] S. Kirkpatrick, C. D. Gelatt, and M. P. Vecchi, Optimization by simulated annealing, *Science* **220**, 671 (1983).
- [26] R. Monasson and R. Zecchina, Statistical mechanics of the random k-satisfiability model, *Phys. Rev. E* **56**, 1357 (1997).
- [27] M. Mézard, T. Mora, and R. Zecchina, Clustering of solutions in the random satisfiability problem, *Phys. Rev. Lett.* **94**, 197205 (2005).
- [28] M. Mézard and G. Parisi, Replicas and optimization, *J. Phys. Lett.* **46**, 771 (1985).
- [29] M. Mézard and R. Zecchina, Random k -satisfiability problem: From an analytic solution to an efficient algorithm, *Phys. Rev. E* **66**, 056126 (2002).
- [30] R. Glauber, Time-dependent statistics of the Ising model, *J. Math. Phys.* **4**, 294 (1963).
- [31] D. Dahmen, H. Bos, and M. Helias, Correlated fluctuations in strongly coupled binary networks beyond equilibrium, *Phys. Rev. X* **6**, 031024 (2016).
- [32] M. Mézard, G. Parisi, and M. Virasoro, *Spin Glass Theory and Beyond (World Scientific Lecture Notes in Physics, Vol 9)* (World Scientific Publishing Company, 1987).
- [33] U.-P. Wen, K.-M. Lan, and H.-S. Shih, A review of hopfield neural networks for solving mathematical programming problems, *European Journal of Operational Research* **198**, 675 (2009).

- [34] P. M. Talaván and J. Yáñez, Parameter setting of the hopfield network applied to tsp, *Neural Networks* **15**, 363 (2002).
- [35] Q. Wang, X. Sun, B. L. Golden, and J. Jia, Using artificial neural networks to solve the orienteering problem, *Annals of Operations Research* **61**, 111 (1995).
- [36] G. Feng and C. Douligeris, Using hopfield networks to solve traveling salesman problems based on stable state analysis technique, in *Proceedings of the IEEE-INNS-ENNS International Joint Conference on Neural Networks. IJCNN 2000. Neural Computing: New Challenges and Perspectives for the New Millennium*, Vol. 6 (IEEE, 2000) pp. 521–526.
- [37] D. Sherrington and S. Kirkpatrick, Solvable model of a spin-glass, *Phys. Rev. Lett.* **35**, 1792 (1975).
- [38] J. R. de Almeida and D. J. Thouless, Stability of the sherrington-kirkpatrick solution of a spin glass model, *Journal of Physics A: Mathematical and General* **11**, 983 (1978).
- [39] A. Misra-Spieldenner, T. Bode, P. K. Schuhmacher, T. Stollenwerk, D. Bagrets, and F. K. Wilhelm, Mean-field approximate optimization algorithm, *PRX Quantum* **4**, 030335 (2023).
- [40] E. Farhi, J. Goldstone, and S. Gutmann, A quantum approximate optimization algorithm applied to a bounded occurrence constraint problem (2015), arXiv:1412.6062 [quant-ph].
- [41] T. Bode and F. K. Wilhelm, Adiabatic bottlenecks in quantum annealing and nonequilibrium dynamics of paramagnons, *Phys. Rev. A* **110**, 012611 (2024).
- [42] M. X. Goemans and D. P. Williamson, Improved approximation algorithms for maximum cut and satisfiability problems using semidefinite programming, *J. ACM* **42**, 1115 (1995).
- [43] S. Diamond and S. Boyd, CVXPY: A Python-embedded modeling language for convex optimization, *J. Mach. Learn. Res.* **17**, 1 (2016).
- [44] M. Lewin, D. Livnat, and U. Zwick, Improved rounding techniques for the max 2-sat and max di-cut problems, in *Integer Programming and Combinatorial Optimization*, edited by W. J. Cook and A. S. Schulz (Springer Berlin Heidelberg, Berlin, Heidelberg, 2002) pp. 67–82.
- [45] A. Ignatiev, A. Morgado, and J. Marques-Silva, PySAT: A Python toolkit for prototyping with SAT oracles, in *SAT* (2018) pp. 428–437.
- [46] A. Ignatiev, A. Morgado, and J. Marques-Silva, Rc2: an efficient maxsat solver, *Journal on Satisfiability, Boolean Modelling and Computation* **11**, 53 (2019).
- [47] M. ApS, *MOSEK Optimizer API for Python. Version 10.2.8* (2024).
- [48] F. Krzakala and L. Zdeborová, Hiding quiet solutions in random constraint satisfaction problems, *Physical review letters* **102**, 238701 (2009).
- [49] N. Mohseni, P. L. McMahon, and T. Byrnes, Ising machines as hardware solvers of combinatorial optimization problems, *Nature Reviews Physics* **4**, 363 (2022).
- [50] F. Cai, S. Kumar, T. Van Vaerenbergh, X. Sheng, R. Liu, C. Li, Z. Liu, M. Foltin, S. Yu, Q. Xia, *et al.*, Power-efficient combinatorial optimization using intrinsic noise in memristor hopfield neural networks, *Nature Electronics* **3**, 409 (2020).
- [51] M. Hizzani, A. Heittmann, G. Hutchinson, D. Dobrynin, T. Van Vaerenbergh, T. Bhattacharya, A. Renaudineau, D. Strukov, and J. P. Strachan, Memristor-based hardware and algorithms for higher-order hopfield optimization solver outperforming quadratic ising machines, in *2024 IEEE International Symposium on Circuits and Systems (ISCAS)* (IEEE, 2024) pp. 1–5.
- [52] A. C. C. Coolen, Statistical mechanics of recurrent neural networks i. statics, ArXiv (2000).
- [53] I. Ginzburg and H. Sompolinsky, Theory of correlations in stochastic neural networks, *Phys. Rev. E* **50**, 3171 (1994).
- [54] A. Renart, J. De La Rocha, P. Bartho, L. Hollender, N. Parga, A. Reyes, and K. D. Harris, The asynchronous state in cortical circuits, *Science* **327**, 587 (2010).

Appendix A: Mapping CSPs to Ising systems

Here we shortly repeat the mapping of MAX- K -SAT problems to Ising systems [26], done in a way such that the number of violated clauses in the CSP matches the energy in the Ising system (we use $K = 2$ throughout this work). We start by identifying spin S_i with variable x_i , where $x_i = 0$ and $x_i = 1$ correspond to $S_i = -1$ and $S_i = +1$, respectively. In the CSP, one aims to minimize the number of violated clauses

$$C_l = \bigvee_{k=1}^K z_{i_k, l},$$

i.e., the number of clauses with value $C_l = 0$. Here the literals z_i are either x_i or their negation $\bar{x}_i = 1 - x_i$. Requiring the number of violated clauses to match the energy of the Ising system, we get

$$E(\mathbf{S}) = \sum_{l=1}^M \delta \left[\sum_{i=1}^N \Delta_{l,i} S_i; -K \right] \quad (\text{A1})$$

as the energy function, where $\delta[a; b] = \delta_{a,b}$ is the Kronecker delta: If all Boolean variables in one clause C_l take the opposite of the value required to make C_l true, one requires $\sum_{i=1}^N \Delta_{l,i} S_i = -K$. For this to hold, one needs that

$$\Delta_{l,i} = \begin{cases} +1 & \text{if } x_i \text{ appears} \\ -1 & \text{if } \bar{x}_i = 1 - x_i \text{ appears} \\ 0 & \text{otherwise} \end{cases}. \quad (\text{A2})$$

Now we notice that

$$\prod_{i=1}^N (1 - \Delta_{l,i} S_i) = \begin{cases} 2^K & \text{if } C_l = 0 \\ 0 & \text{if } C_l = 1 \end{cases} \quad (\text{A3})$$

which we use to rewrite the energy

$$E(\mathbf{S}) = \frac{1}{2^K} \sum_{l=1}^M \prod_{i=1}^N (1 - \Delta_{l,i} S_i). \quad (\text{A4})$$

The product can be expanded to

$$\prod_{i=1}^N (1 - \Delta_{l,i} S_i) = 1 + \sum_{R=1}^K (-1)^R \sum_{i_1 < i_2 < \dots < i_R} \Delta_{l,i_1} \Delta_{l,i_2} \dots \Delta_{l,i_R} S_{i_1} S_{i_2} \dots S_{i_R} \quad (\text{A5})$$

$$= 1 - \sum_i \Delta_{l,i} S_i + \frac{1}{2} \sum_{i \neq j} \Delta_{l,i} \Delta_{l,j} S_i S_j \mp \dots \quad (\text{A6})$$

Restricting to $K = 2$ yields the energy function (1) where the parameters are

$$H_i = \frac{1}{4} \sum_{l=1}^M \Delta_{l,i} \quad (\text{A7})$$

$$J_{ij} = \frac{1}{4} (\delta_{ij} - 1) \sum_{l=1}^M \Delta_{l,i} \Delta_{l,j}. \quad (\text{A8})$$

Appendix B: Implementation

Our code will be available at Zenodo upon acceptance of this manuscript.

1. Generation of random CSPs

Throughout our manuscript, we refer to random MAX-2-SAT problems as random CSPs. The clauses are generated by picking two random spins and assigning two random values to the spins (both uniformly) while respecting the following conditions:

1. Each variable appears at least once in a clause. If this would not be the case, the value assigned to these disconnected variables would be irrelevant and the problem is reduced to a problem with $N - N_{\text{disconnected}}$ variables.
2. Each clause contains two distinct variables. If both variables of one clause are the same, either the truth value will be independent of the variable's value (for $x_i \vee \tilde{x}_i$) which would have no impact on the difficulty of the CSP, or the clause will be reducible to length one, violating our prerequisite to only have length two clauses.
3. All clauses have to be distinct from one another.

Appendix C: Hopfield networks in simplified notation

In the original work [11] the Hopfield network was written in the form

$$C_i \frac{du_i(t)}{dt} = -\frac{u_i(t)}{R_i} + T_{ij}V_j(t) + I_i \quad (\text{C1})$$

$$u_i(t) = g_i^{-1}(V_i(t)). \quad (\text{C2})$$

The network equations are biologically motivated, u_i and V_i play the role of input and output to/from neuron i , respectively, and g_i denotes the input-output characteristic. Moreover, C_i is the input capacitance of the cell membrane and R_i the transmembrane resistance. Finally, T_{ij}^{-1} denotes the impedance between outputs V_j and neuron i , and I_i is a (time-independent) input current. For our work, we rename $R_i = \beta$, $u_i \rightarrow \mu_i/\beta$, $C_i \rightarrow \tau/\beta$, $T_{ij} \rightarrow J_{ij}$ and $I_i \rightarrow H_i$ and choose $g_i = \tanh$ which is a standard choice for practical use of the Hopfield network. In this notation, the Hopfield dynamics take the form (2).

Appendix D: Derivations of Glauber-based solvers

In the following, for completeness, we recapitulate some aspects of the derivations of the Glauber dynamics [30], in particular the choice of gain function F that is required for the system to sample from the correct Ising system, specified by the energy in equation (1). Furthermore, we present a systematic derivation of the different Glauber-based CSP solvers based on a cumulant expansion [31].

1. Gain function

When evolving the Glauber dynamics, due to the symmetry in couplings, the spin system will eventually reach equilibrium at which the probability of leaving a state is the same as entering a state [52]

$$p(\mathbf{S}_{i-})F_i^+(\mathbf{S}\setminus S_i) = p(\mathbf{S}_{i+}) \underbrace{(1 - F_i^+(\mathbf{S}\setminus S_i))}_{=F_i^-(\mathbf{S}\setminus S_i)}. \quad (\text{D1})$$

In an equilibrium state, the joint probability distribution is proportional to the Boltzmann factor

$$p(\mathbf{S}) \propto e^{-\beta E[\mathbf{S}]}. \quad (\text{D2})$$

When we plug in the energy Hamiltonian (1) we can calculate the ratio of $p(\mathbf{S}_{i-})$ and $p(\mathbf{S}_{i+})$ as

$$\frac{p(\mathbf{S}_{i-})}{p(\mathbf{S}_{i+})} = \frac{F_i^-(\mathbf{S}\setminus S_i)}{F_i^+(\mathbf{S}\setminus S_i)} = \frac{\exp(-\beta E[\mathbf{S}_{i-}])}{\exp(-\beta E[\mathbf{S}_{i+}])} \quad (\text{D3})$$

$$= \frac{\exp(-\beta h_i)}{\exp(\beta h_i)} \quad (\text{D4})$$

$$= \exp(-2\beta h_i). \quad (\text{D5})$$

and solve (D1) for $F_i^+(\mathbf{S}\setminus S_i)$ to obtain the gain function

$$F_i^+(\mathbf{S}\setminus S_i) = \frac{1}{1 + e^{-2\beta h_i}} = \frac{1}{2} \tanh(\beta h_i) + \frac{1}{2}.$$

Here $h_i = H_i + \sum_j J_{ij} S_j(t)$ denotes the local field, i.e. the total magnetic field that spin i experiences.

2. Mean-field approximation

The mean values of the spins are defined by

$$m_i(t) = \sum_{\{\mathbf{S}\}} S_i p(\mathbf{S}, t). \quad (\text{D6})$$

By employing the master equation (3) we can calculate the time derivative of the mean as

$$\tau \frac{d}{dt} m_i(t) = \sum_{\{\mathbf{S}\}} S_i \tau \frac{d}{dt} p(\mathbf{S}, t) \quad (\text{D7})$$

$$= \sum_{\{\mathbf{S}\}} \sum_{j=1}^N S_i S_j (p(\mathbf{S}_{j-}) F_j^+(\mathbf{S}\setminus S_j) - p(\mathbf{S}_{j+}) F_j^-(\mathbf{S}\setminus S_j)). \quad (\text{D8})$$

For terms with $i \neq j$, the sum over all configurations cancels every term, leaving

$$\tau \frac{d}{dt} m_i(t) = \sum_{\{\mathbf{S}\}} (p(\mathbf{S}_{i-}) F_i^+(\mathbf{S}\setminus S_i) - p(\mathbf{S}_{i+}) F_i^-(\mathbf{S}\setminus S_i)). \quad (\text{D9})$$

Using $F_i^-(\mathbf{S}\setminus S_i) = 1 - F_i^+(\mathbf{S}\setminus S_i)$ yields

$$\tau \frac{d}{dt} m_i(t) = \sum_{\{\mathbf{S}\}} p(\mathbf{S}_{i-}, t) F_i^+(\mathbf{S}\setminus S_i) + p(\mathbf{S}_{i+}, t) F_i^+(\mathbf{S}\setminus S_i) - p(\mathbf{S}_{i+}, t) \quad (\text{D10})$$

$$= \sum_{\{\mathbf{S}\}} 2 \left(p(\mathbf{S}, t) F_i^+(\mathbf{S}\setminus S_i) - \frac{1 + S_i}{2} p(\mathbf{S}, t) \right) \quad (\text{D11})$$

$$= 2 \langle F_i^+(\mathbf{S}\setminus S_i) \rangle - 1 - \langle S_i \rangle. \quad (\text{D12})$$

To get from (D10) to (D11) we used the fact that

$$\sum_{\{\mathbf{S}\}} f(\mathbf{S}) p(\mathbf{S}_{i\pm}, t) = \sum_{\{\mathbf{S}\}} 2f(\mathbf{S}) \left(\frac{1 \pm S_i}{2} p(\mathbf{S}, t) \right), \quad (\text{D13})$$

for an arbitrary function $f(\mathbf{S})$. Now we can use the explicit form of $F_i(\mathbf{S}\setminus S_i)$ to obtain

$$\tau \frac{d}{dt} m_i(t) + m_i(t) = \langle 2F_i^+(\mathbf{S}\setminus S_i) - 1 \rangle \quad (\text{D14})$$

$$= \langle \tanh(\beta x_i) \rangle. \quad (\text{D15})$$

At lowest order, i.e. neglecting all fluctuations in x_i , this matches the result of the Hopfield networks (see Appendix E)

$$\tau \frac{d}{dt} m_i(t) = -m_i + \tanh(\beta \mu_i). \quad (\text{D16})$$

3. Inclusion of spin variances

Now we want to include also the spin variances. To do so we can make use of the fact that the variances of total inputs

$$\sigma_i^2 = \langle h_i^2 \rangle - \langle h_i \rangle^2 = \sum_{j,k} J_{ij} J_{ik} (\langle S_j S_k \rangle - \langle S_j \rangle \langle S_k \rangle) \quad (\text{D17})$$

$$\approx \sum_j J_{ij} J_{ij} (1 - \langle S_j \rangle \langle S_j \rangle) + \sum_{j \neq k} J_{ij} J_{ik} (\langle S_j \rangle \langle S_k \rangle - \langle S_j \rangle \langle S_k \rangle) \quad (\text{D18})$$

$$= \sum_j J_{ij}^2 (1 - m_j^2) \quad (\text{D19})$$

are a direct function of the means m_i when covariances between neurons are neglected. At lowest order the local field h_i is by the central limit theorem Gaussian distributed [31] so the equation becomes

$$\tau \frac{d}{dt} m_i(t) = -m_i + \langle \tanh(\beta h_i) \rangle_{\mathcal{N}(\mu_i, \sigma_i)}. \quad (\text{D20})$$

4. Including spin covariances

To include spin covariances we first calculate the time derivative of the second moment $\langle S_i S_j \rangle$ for $i \neq j$ only since $\langle S_i^2 \rangle = 1$. To simplify the notation we introduce the abbreviation $\phi_i(\mathbf{S} \setminus S_i) := p(\mathbf{S}_{i-}) F_i^+(\mathbf{S} \setminus S_i) - p(\mathbf{S}_{i+}) F_i^-(\mathbf{S} \setminus S_i)$ for the probability flux that was already mentioned in the introduction of the Glauber dynamics [31, 53, 54]:

$$\tau \frac{d}{dt} \langle S_i S_j \rangle = \sum_{\{\mathbf{S}\}} S_i S_j \tau \frac{d}{dt} p(\mathbf{S}, t) \quad (\text{D21})$$

$$\stackrel{\text{eq.(3)}}{=} \sum_{\{\mathbf{S}\}} \sum_{k=1}^N S_i S_j S_k \phi_k(\mathbf{S} \setminus S_k, t) \quad (\text{D22})$$

$$\stackrel{i \neq j}{=} \sum_{\{\mathbf{S}\}} \sum_{k \neq i, j} S_i S_j S_k \phi_k(\mathbf{S} \setminus S_k, t) + \underbrace{S_j^2}_{=1} S_i \phi_j(\mathbf{S} \setminus S_j, t) + \underbrace{S_i^2}_{=1} S_j \phi_i(\mathbf{S} \setminus S_i, t) \quad (\text{D23})$$

$$= \sum_{\{\mathbf{S}\}} (S_i \phi_j(\mathbf{S} \setminus S_j, t) + S_j \phi_i(\mathbf{S} \setminus S_i, t)). \quad (\text{D24})$$

Plugging in the flux yields

$$\sum_{\{\mathbf{S}\}} S_i \phi_j(\mathbf{S} \setminus S_j, t) = \sum_{\{\mathbf{S}\}} S_i (F_j^+(\mathbf{S} \setminus S_j) (p(\mathbf{S}_{j+}, t) + p(\mathbf{S}_{j-}, t)) - p(\mathbf{S}_{j+}, t)) \quad (\text{D25})$$

$$\stackrel{\text{eq.(D13)}}{=} \sum_{\{\mathbf{S}\}} S_i (2F_j^+(\mathbf{S} \setminus S_j) p(\mathbf{S}, t) - (1 + S_j) p(\mathbf{S}, t)) \quad (\text{D26})$$

$$= \langle S_i (2F_j^+(\mathbf{S} \setminus S_j) - 1) \rangle - \langle S_i S_j \rangle \quad (\text{D27})$$

$$= \langle S_i G_k(\mathbf{S}) \rangle - \langle S_i S_k \rangle, \quad (\text{D28})$$

where $G_i(\mathbf{S}) = 2F_i^+(\mathbf{S} \setminus S_i) - 1 = \tanh(\beta x_i)$. So in total we have

$$\tau \frac{d}{dt} \langle S_i S_j \rangle = \langle G_i(\mathbf{S}) S_j \rangle + \langle G_j(\mathbf{S}) S_i \rangle - 2 \langle S_i S_j \rangle. \quad (\text{D29})$$

The time derivative of the covariance then follows as

$$\tau \frac{d}{dt} c_{ij} = \langle G_i(\mathbf{S}) S_j \rangle + \langle G_j(\mathbf{S}) S_i \rangle - 2 \langle S_i S_j \rangle - \langle S_i \rangle (\langle G_j(\mathbf{S}) \rangle - \langle S_j \rangle) - \langle S_j \rangle (\langle G_i(\mathbf{S}) \rangle - \langle S_i \rangle) \quad (\text{D30})$$

$$= \langle G_i(\mathbf{S}) \delta S_j \rangle + \langle G_j(\mathbf{S}) \delta S_i \rangle - 2c_{ij}, \quad (\text{D31})$$

where $\delta S_i = S_i - \langle S_i \rangle$ is the centralized variable. We can now write $\langle G_i(\mathbf{S})S_j \rangle$ with the Fourier transform of $G_i(\mathbf{S}) = G_i(\beta x_i)$ as [31]

$$\langle G_i(\mathbf{S})S_j \rangle = \frac{1}{2\pi} \int d\omega \hat{g}(\omega) \langle \exp(i\omega\beta x_i) S_j \rangle \quad (\text{D32})$$

$$= \frac{1}{2\pi} \int d\omega \hat{g}(\omega) \left\langle \exp \left(i\omega\beta \left(\sum_k J_{ik} S_k + H_i \right) \right) S_j \right\rangle \quad (\text{D33})$$

$$= \frac{1}{2\pi} \int d\omega \hat{g}(\omega) e^{i\omega\beta H_i} \left. \frac{\partial}{\partial j_j} \langle \exp(\mathbf{j}^T \mathbf{S}) \rangle \right|_{j_j = i\omega\beta J_{ij}}. \quad (\text{D34})$$

Here we introduced the source $j_k = i\omega\beta J_{ik}$. We can identify the moment generation function $\varphi(\mathbf{j}) = \langle \exp(\mathbf{j}^T \mathbf{S}) \rangle$ and express it by the cumulant generating function $\Phi(\mathbf{j}) = \ln \varphi(\mathbf{j})$

$$\langle G_i(\mathbf{S})S_j \rangle = \frac{1}{2\pi} \int d\omega \hat{g}(\omega) e^{i\omega\beta H_i} \left. \frac{\partial}{\partial j_j} e^{\Phi(\mathbf{j})} \right|_{j_j = i\omega\beta J_{ij}} \quad (\text{D35})$$

$$= \frac{1}{2\pi} \int d\omega \hat{g}(\omega) e^{i\omega\beta H_i} \langle \exp(\mathbf{j}^T \mathbf{S}) \rangle \left. \frac{\partial}{\partial j_j} \Phi(\mathbf{j}) \right|_{j_j = i\omega\beta J_{ij}}. \quad (\text{D36})$$

Now we do a Gaussian approximation by assuming all cumulants higher than two are zero, i.e.

$$\Phi(\mathbf{j}) = \sum_k m_k j_k + \frac{1}{2} \sum_{k,l} c_{kl} j_k j_l. \quad (\text{D37})$$

Plugging that into (D36) yields [31]

$$\langle G_i(\mathbf{S})S_j \rangle \simeq \frac{1}{2\pi} \int d\omega \hat{g}(\omega) \langle \exp(i\omega\beta x_i) \rangle \left(m_j + \sum_k i\omega\beta J_{ik} c_{kj} \right), \quad (\text{D38})$$

where we can identify the moment generating function $\langle \exp(i\omega\beta x_i) \rangle$ of the field x_i . As for the case with only spin variances, we assume x_i to be Gaussian distributed so

$$\langle \exp(i\omega\beta x_i) \rangle = \exp \left(i\omega\beta \mu_i + \frac{1}{2} (i\omega\beta \sigma_i)^2 \right). \quad (\text{D39})$$

We can get the factor $i\omega\beta$ in the covariance term by differentiating this moment generating function by μ_i . Therefore we get

$$\langle G_i(\mathbf{S})S_j \rangle \simeq \frac{1}{2\pi} \int d\omega \hat{g}(\omega) \left(m_j + \sum_k J_{ik} c_{kj} \frac{\partial}{\partial \mu_i} \right) \langle \exp(i\omega\beta x_i) \rangle \quad (\text{D40})$$

$$= \langle G_i(\mathbf{S}) \rangle \langle S_j \rangle + \sum_k J_{ik} c_{kj} \frac{\partial}{\partial \mu_i} \langle G_i(\mathbf{S}) \rangle, \quad (\text{D41})$$

and with the definition of the susceptibility $\chi_i = \frac{\partial}{\partial \mu_i} \langle G_i(\mathbf{S}) \rangle$ we find

$$\langle G_i(\mathbf{S}) \delta S_j \rangle \simeq \chi_i \sum_k J_{ik} c_{kj}. \quad (\text{D42})$$

Thereby, the differential equation that describes the time evolution of the covariance is (7b) with

$$h_i(m(t), c(t)) = \sum_k (\chi_i(t) J_{ik} c_{kj}(t) + \chi_j(t) J_{jk} c_{ki}(t)) - 2c_{ij}(t). \quad (\text{D43})$$

Here $\chi_i(t)$ is a time-dependent susceptibility, which depends on $m(t)$ and $c(t)$. The variances of the total input are

described by (7c) with

$$f_i(m(t), c(t)) = \langle h_i^2 \rangle - \langle h_i \rangle^2 \quad (\text{D44})$$

$$= \sum_{j,k} J_{ij} J_{ik} c_{jk}(t) \quad (\text{D45})$$

$$= \sum_j J_{ij}^2 (1 - m_j^2(t)) \quad (\text{D46})$$

$$+ \sum_{j \neq k} J_{ij} J_{ik} c_{jk}(t) \quad (\text{D47})$$

For a stationary state ($\frac{d}{dt} c_{ij} = 0$), the equation self-consistency equation for the covariances becomes

$$c_{ij} = \frac{1}{2} \sum_k (\chi_i J_{ik} c_{kj} + \chi_j J_{jk} c_{ki}). \quad (\text{D48})$$

Appendix E: Equivalence of mean-field Glauber dynamics and Hopfield networks

Here we show that the Hopfield dynamics stated in (2) and the mean field dynamics in (4a) and (4b) are equivalent. We start with taking the time derivative of (4b) (multiplied with τ) to calculate

$$\tau \frac{d\mu_i}{dt} = \tau \sum_j J_{ij} \frac{dm_j}{dt}. \quad (\text{E1})$$

Insertion of (4a) on the right hand side yields

$$\frac{d\mu_i}{dt} = \sum_j J_{ij} (-m_j + \tanh(\beta \mu_j)) \quad (\text{E2})$$

$$= H_i - \mu_i + J_{ij} \tanh(\beta \mu_j) \quad (\text{E3})$$

where we used (4b) again to replace $\sum_j J_{ij} m_j = \mu_i - H_i$. This is exactly equation (2).

Appendix F: Additional plots

Here we show additional plots to complement our analysis in the main text. Figure A7 shows the performance comparison of Glauber dynamics and the Hopfield-network dynamics over a larger range of clause densities α compared to Figure 1c). While the performance difference is most clear for small α , we find the Glauber dynamics to outperform the Hopfield network for all α .

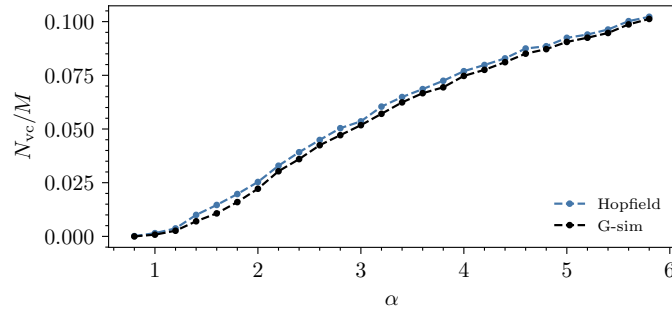


Figure A7. Performance of Glauber dynamics and Hopfield network for a wider range of α compared to Figure 1c. Parameters: $N = 400$, $T = 0.1$.

In Figure 2 we compared the simulated Glauber dynamics with the mean-field, variance and covariance predictions for two randomly chosen spins, from which we conclude that the mean-field approximation is not sufficient for small

temperatures. To corroborate this conclusion, we show the deviation between Glauber dynamics and approximations for the five spins with the strongest deviations in Figure A8; the spins are individually chosen for each approximation. While the mean-field deviation is small for high temperatures, we observe strong deviations for small temperatures and both CSPs and SK couplings. In contrast, the variance and covariance solver both provide accurate descriptions of the simulated dynamics in all cases.

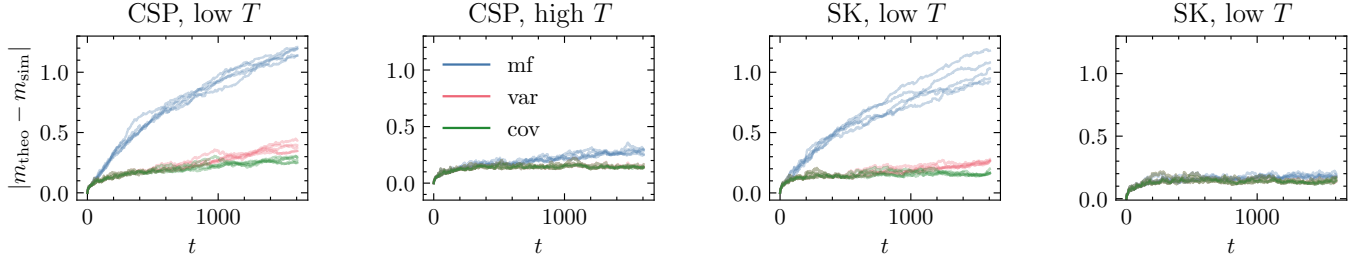


Figure A8. Deviation between Glauber simulation magnetizations and the predictions of the mean-field, variance and covariance solver for CSP and SK couplings shown for the 5 spins with the highest deviation. High T is $T = 1$ and low T is $T = 0.1$. Parameters: $N = 400$, $\alpha = 3$.

Figure 5c compares the variance prediction obtained by the different theoretic solvers (G-var and G-cov) with the results from the simulation for one random CSP instance. In A9 we show the difference between the variance prediction and the result from the simulation averaged over different instances and across different clause densities to demonstrate that the covariance solver universally matches the simulation better than the variance solver. Taking into account spin correlations results in better agreement between theory and simulation. The magnitude of this improvement is not dependent on α , which shows that correlations play a role for all tested clause densities.

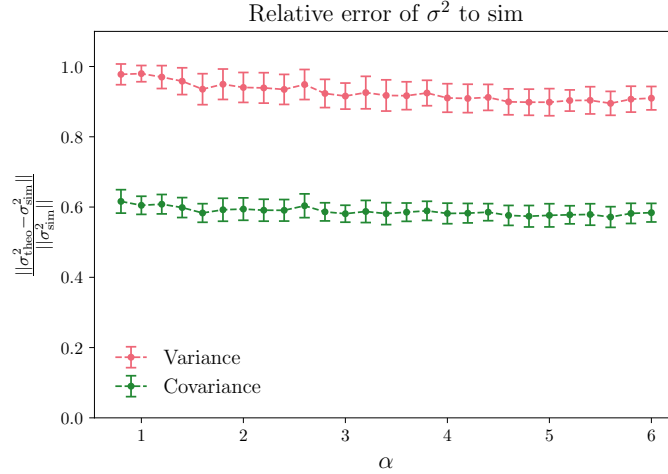


Figure A9. Covariance versus variance solver. Relative norm of the difference between theoretical and simulated variance plotted as a function of clause density α . Statistics was calculated over 50 different random CSPs per α .